RSC Advances

ROYAL SOCIETY OF CHEMISTRY

www.rsc.org/advances

A Performance Study on Electrocoating Process with CuZnAl Nano-Catalyst for Methanol Steam Reformer: Effect of Time and Voltage

Masoud Mahmoudizadeh [1], Abdullah Irankhah [1,*], Reza Irankhah[2]

[1] Hydrogen and Fuel Cell Research Laboratory, Department of Chemical Engineering, Faculty of Engineering, University of Kashan, Kashan, Iran.
Email: Irankhah@kashanu.ac.ir
[2] Department of Ceramic, Materials and Energy Research Center, Tehran, 14155-4777, Iran.

Abstract

Coated microreactors as an alternative strategy are to enhance performance of desired objects especially portable devices and fuel cell applications. To successfully employ catalyst onto microreactors, study of coating methods is an essential need. In this paper, high potential electrophoretic deposition technique was used to coat CuZnAl catalyst on stainless steel. The prime aim of this examination is to determine the effects of time and voltage of coating on catalyst performance. First, the CuZnAl catalyst was synthesized by co-precipitation method to catalyze the methanol steam reforming. The powder was characterized by X-ray diffraction, ICP-OES and BET analyses. Second, based on the deposition time, methanol conversion was improved by increase in time of coating to 4 minutes followed by a bit fall of both conversion and deposition weight for time of 5 minutes. Third, it was found increase in voltage from 60 to 140 V enhanced conversion while no deposition was achieved for higher voltages. The optimum conditions of 140 V and 4 minutes resulted in nearly full methanol conversion and

CO selectivity of 4.91% at 270 °C. Finally, the microreactor possessed higher activity than that of packed bed one. The coated layers were analyzed by field-emission scanning electron microscope.

Keywords: Electrophoretic Deposition, CuZnAl Catalyst, Hydrogen, Methanol Steam Reforming, Microreactor, PEM Fuel Cell,

1 Introduction

Nowadays, industrial applications of hydrogen including oil desulphurization, methanol, ammonia synthesis, water gas shift, and hydrogenation of chemical agents highlight its situation as a pivotal agent [1, 2]. Regard to reforming as a critical approach of hydrogen production, liquid energy carriers like methanol, dimethyl ether, and gasoline are appropriate candidates for on-board applications [3, 4]. Methanol is broadly used for hydrogenous fuel processor especially mobile applications because it could be reformed through a Cu-based catalyst in range of 200-300 °C [5]. Methanol reforming takes into account several advantages such as easy storage, transport, and conversion with a microreformer. Moreover, attractive and promising results of methanol steam reforming (MSR) lead especial insight into this reaction. It is performed by following reactions:

$$CH_3OH+H_2O=CO_2+3H_2 \qquad \Delta H\,°298\ K = +49.7 \qquad kJ\ mol^{-1} \qquad (1)$$

$$CO+H_2O=CO_2+H_2 \qquad \Delta H\,°298\ K = -41.2 \qquad kJ\ mol^{-1} \qquad (2)$$

$CH_3OH=CO+3H_2$ $\Delta H\,°298\ K = +90.7$ kJ mol^{-1} (3)

Where the reactions 1, 2 and 3 represent MSR, water gas shift (WGS) and decomposition of methanol (DM), respectively [6]. To gain more effective hydrocarbon reforming, optimization of all parameters attributed to both catalyst and reactor design are crucial owing to their influential physiochemical properties. Coated metal-based microreactors represent significant advantages such as higher surface to volume ratio, smaller mean distance of the specific fluid volume to the reactor walls, and better heat and mass transfer that facilitate integrating with fuel processor systems [7]. In this way, potential to coat the thin layers of reforming catalysts onto the metal microreactors is a crucial factor for this field. Typically, sol-gel, electrophoretic deposition (EPD), electrochemical deposition, and electroless plating are employed for liquid phase coating, whereas chemical and physical vapor deposition, and also plasma spraying are used for gas phase coating [8]. In this regard, liquid phase methods are preferred owing to capacity of previously prepared powders coating.

EPD is broadly employed to form a favorable ceramic layer [9-11], catalyst layer [12, 13], solid oxide fuel cells membrane [14, 15], or even porous membrane [16, 17]. It is a well-known technique that is simultaneously performed by two processes of the charged particles migration in suspension impressed by an electric

field between two electrodes (electrophoresis), and also particle deposition onto an electrode (electrocoagulation) [13]. Typically, EPD represents significant advantages such as simple procedure, low cost equipment, low deposition time, high controllable thickness of coating, and co-deposition of various material [18-20]. EPD is generally consisted of two sets of factors; (i) those based on suspension parameters; and (ii) those related to the physical parameters during the procedure such as voltage, time, and etc. [13].

In this study we examined the cathodic EPD of CuZnAl catalyst on stainless steel to produce hydrogen from methanol steam reforming reaction. Physical properties of voltage and time of EPD procedure were evaluated to find methanol conversion dependency to the coating parameters. The coated palates were successfully characterized and reacted to determine the optimum case.

2 Experimental

2.1 Reactor Design

A flat-plate stainless steel (SUS304) microreactor was designed. The microstructures (L=108, W=1, D=0.3 mm) were machined by computerized numerical control (CNC). The both covering plates were machined to increase the surface to volume ratio, and to direct the flow path on the catalyst layer. The coated palates were sandwiched between the covering plates, and the housing

structure was finally sealed by graphite gasket and bolts. The plates and reformer design are shown in Figure 1.

2.2 Catalyst Preparation

Cu-Zn-Al catalyst was prepared by co-precipitation method. First, an aqueous solution of cupric nitrate trihydrate ($Cu(NO_3)_2.3H_2O$), zinc nitrate tetrahydrate $Zn(NO_3)_2.4H_2O$, and aluminium nitrate nonahydrate $Al(NO_3)_3.9H_2O$ with molarity of 0.5 M was prepared. The prepared solution was heated up to 60 ºC. In the next step, the Na_2CO_3 solution (0.2 M) was added dropwise to adjust the pH around 7. After precipitation, the slurry temperature was fixed at 60 °C for a certain time of 3 h under continuous stirring. After that, the cooled mixture was filtered and washed with warm D.I water to remove the ions. The prepared cake was dried at 110 °C for 18 h and calcined at 350 °C for 4 h in air atmosphere with heating rate of 3 °C min^{-1} [21]. The chemical composition of synthesized catalyst was determined by inductively coupled plasma-optical emission spectrometer (ICP-OES, ARL – Model 3410 apparatus) after dissolution of the catalyst in hydrochloric acid, which is given in table 1.

2.3 Slurry Preparation

First, the synthesized catalyst was milled for 10 minutes (due to low initial particle size, short time of milling was selected) at a speed of 250 rpm and then was sieved

via a fine screen mesh (No. 400), particle size less than 38 μm. It effectively improves the suspension stability. Each suspension was included isopropanol (organic medium), nanocatalyst of CuZnAl (powder content), and additive agent of polyethylenimine (PEI). It was contained 75 g/l of nanocatalyst in isopropanol, and 0.6 wt. % of additive agent. PEI was used as polymeric agent to create a strict bonding and to increase stability, control of deposition, and drying rate. The procedure was completed by 15 minutes strongly stirring, and then 15 minutes sonification in an ultrasonic bath (1200M-Soltec). Several physical-chemical properties of the slurry and coating process were assessed to obtain optimal conditions of a desirable case. All cases are illustrated in Table 2.

2.4 Substrate treatment

Stainless steel (SUS304) plates were cut to 32 L and 22 W (mm) in dimension, exposed area of 7.04 cm^2. Prior to the deposition, the substrate plates were mechanically polished from 800 to 1200 grit emery papers. They were then washed with rinsing agent and D.I water followed by ultrasonic treatment with acetone for 5 minutes. Consequently, they were dried at room temperature followed by keeping in a desiccator.

2.5 Electrophoretic Deposition Methodology

The coating was carried out using a constant voltage power supply unit (SPS-900NP-Navasanpardaz). The electric current was also recorded using a digital multimeter (Haoyue, China). Electrophoretic deposition was conducted in a 120 ml beaker with conventional three electrodes cell system. The electrodes were mounted at a distance of 15 mm. The stainless plates with the same size of cathode were considered for anode, as well. An overview of coating procedure and EPD set-up are shown in Figure 2.

2.6 Catalytic Layer Characterization

The crystalline catalyst structure was characterized by XRD using a diffractometer (PANalytical X'pert-Pro) and a Cu-Kα monochromatized radiation as the X-ray source with a Ni filter in the 2θ range of 10-80º. The crystallite sizes could be calculated from the widths of the X-ray diffraction peaks using the Debye-Scherer's equation:

$$D = \frac{0.9\,\lambda}{\beta \cos\theta} \qquad (4)$$

Where D is the crystal size of the powder, λ the X-ray wavelength (0.15405 nm), β the full width at half maximum (FWHM) of the diffraction peak (radian), and θ is the diffraction angle at the peak maximum. Crystalline phases were recognized according to the joint committee on powder diffraction standards (JCPDS) database. The catalyst layer surface morphology was analyzed by field emission

scanning electron microscopy (FESEM, MIRA3 TESCAN). An accelerating voltage of 15 kV, a working distance of 25 mm was used. A gold coating was applied to the specimens to avoid ionization under the electron beam in FESEM. Brunauer-Emmett-Teller (BET) method was used to measure the surface area of the prepared catalysts. Lattice parameters (a, b and c) were calculated from the diffraction pattern at around 2θ=32º and 44º through the relating expression for hexagonal structure.

$$\frac{1}{d_{hlk}^2} = \frac{4}{3}.\frac{(h^2 + k^2 + hk)}{a^2} + \frac{l^2}{c^2} \qquad (5)$$

2.7 Methanol Steam Reforming

MSR over CuZnAl catalyst was conducted in a flat-plate microreactor, as shown in Figure 1. The microreactor was located in an electrical heater to supply the reaction heat. Besides, a quartz tube-shape reactor (16 mm outer diameter) was used to compare to the microreactor performance. It was also placed into a cylindrical furnace. A k-type thermocouple was attached inside the covering plate to control the reaction temperature. Prior to MSR, the catalyst activation was performed as follow: the catalyst-coated plates were reduced at 300 °C for 4 h

under H_2 atmosphere with a flow rate of 30 ml min^{-1} to reduce copper oxide into Cu^0 [22]. In case of reforming, methanol-water mixture with ratio of 1:1.3 was fed to the evaporator section, containing a tubular segment filled with inert alumina granules with temperature of 150 °C, and then supplied into the reaction section by a syringe pump (japan, jp500). A cold trap was located after output to condense and separate the residual methanol and water. A gas chromatograph (GC-Shimadzu 8A) equipped with a thermal conductivity detector and a carbosieve column was used to analyze the reformed compositions. Moreover, the output flow rate measured by a soap-bubble flow meter. In all experiments, depending on deposition weight, flowrates of 0.1 to 0.6 ml h^{-1} and 7 to 20 ml min^{-1} were considered for pump and Ar, respectively. It is required to make an equal gas hourly velocity (GHSV) of 23000 h^{-1} and ratio of argon/pump=33.33 for all cases. In this paper, range of 230-270 °C was selected as operating temperature. The methanol conversion X_{MeOH}, and yield of hydrogen (Y_{H_2}) were calculated by the following equations, respectively.

$$X_{MeOH} = \frac{F\left(y_{CO} + y_{CO_2}\right)}{22.4 \times \vartheta_{MeOH,in}} \times 100\% \quad (6)$$

$$Y_{H_2} = \frac{\vartheta_{H_2}}{3 \times \vartheta_{MeOH,in}} \times 100\% \quad (7)$$

Where F (mol.s^{-1}) is the normal flow rate of effluent gas. ϑ_{H_2} and $\vartheta_{MeOH,in}$ denote the molar flowrate of H_2 obtained in the output and the methanol molar flowrate fed into the microreactor, respectively.

3 Results and Discussion

3.1 XRD Analysis

Figure 3 shows the XRD patterns of powder and coated layer in different states at 2θ=10-70º. A strong peaks at 2θ=36.15º and a low intensity peak at 2θ=38.76º have been appeared that represent the CuO (monoclinic phase of CuO, JCPDS 01-080-1268). The mentioned peaks include (-1, 1, 1) and (1, 1, 1) structure, respectively. Moreover, the peaks at 2θ = 31.81, 34.64, 36.15, 56.76º are related to ZnO (hexagonal phase of ZnO, JCPDS 01-079-0207). The main peak of ZnO at 2θ=36.15º overlaps with the monoclinic phase of CuO. Not any strong peak attribute to the CuO was separately detected, although high Cu loading had selected. It could be related to the micro crystalline structure or coverage by the strong and wide peaks of ZnO. In case of Al_2O_3, not any considerable peak was found. It might be cause of low crystallinity or low temperature of calcination. Amorphous phase of Al_2O_3 causes higher BET and more catalyst stability against Cu particle sintering. Temperature of 350 ºC was selected as both calcination temperature of synthesizing and coating [23]. According to the results of Table 1, it

could be observed that the crystallinity is grown for the used case. The growth of ZnO crystallinity might attribute to its structural changes that will affect the interaction between copper and zinc oxide [24]. Moreover, in case of Cu sintering, the tendency depends on the interaction with the ZnO matrix and the Cu/Zn ratio [25]. Moreover, for coated cases, the patterns show additional peaks of stainless steel 304 which mainly include Fe and Fe-Ni at 2θ=44.35, 64.52º and 2θ=43.49, 74.54º, respectively.

3.2 Time of EPD

Figure 4 shows the top view FESEM images of coated layer for different time of EPD (2, 4 and 5 minutes). The results display surface morphology variation with the EPD time. Although no high differences are shown, by-effects like crack formation influence the final efficiency, and it is required to investigate the effect of the time. An almost homogenous layer containing low-intensity cracks was observed for time of 2 minutes. The electric field is decreased during time of deposition due to increase in electric resistivity of the layer. Therefore, smaller particles could deposit, when the shear stress is decreased at long time of EPD. Local agglomeration on the surface might be contributed to the smaller particles, as shown in Figure 4. In case of crack formation, increase in the time could raise layer thickness, that it reasonably affects crack formation. Increase in resistivity of layer by growth of the thickness influences rate of evaporation and drying [26].

Figure 5 plots weight of the coated layers against the time of EPD within range of 2 to 5 minutes. At the initial time of deposition, both methanol conversion and weight distribution are proportional to the deposition time. As it continues to 4 minutes, a linear appearance is reached, while further time of EPD leads a slight fall of both conversion and deposition weight. Figure 6 shows that raising the temperature results in higher methanol conversion. The conversion is reached to 98.8 % for time of 4 minutes at 270 °C. It is increased from 83.5 to 98.8 % at 270 °C, as the deposition time is differed from 2 to 4 minutes. Besides, packed-bed reactor was also compared to the coated cases that its details are illustrated in Table 3. It could be found that weight of deposition broadly influences the conversion. More active sites is reached with higher deposition. However, after time of 4 minutes, a decrease in the conversion is revealed. In case of CO formation, a suggested mechanism for CO formation is a consecutive production by reverse water gas shift reaction. It is obvious which the reverse water-gas shift is more active in higher temperature [27-29]. The CO concentration depends on the contact time in this mechanism [30]. The higher methanol conversion leads more CO content in the output [31]. CO selectivity could be indirectly linked to time of EPD through this investigation.

Figure 7 demonstrates the current density against time of deposition. The electrophoretic current is crucial for determination of the deposition rate [32]. The

plot is correspondingly decreased during the time of deposition which indicates rate of deposition loss. This is strongly related to the resistivity of the formed layer.

3.3 Effect of Voltage

Figure 5 displays deposition weight as function of applied voltage. It is noticeable, that the increase in applied voltage up to 140 V raises the weight of deposition. However, the weight of deposition suddenly fell at voltages higher than 140 V for the time of 4 minutes, so that no deposition was occurred. This evaluation could be described by following equation. It expresses that higher voltage intensifies the average velocity of CuZnAl particles [32]:

$$V = \mu_e E$$

Where V express the particle velocity (m s^{-1}), μ_e the electrophoretic mobility (m^2 s^{-1} v^{-1}) and E the applied electric field (v m^{-1}). According to the equation, the particles move fast so that a regular arrangement could not formed. Figure 8 shows the surface of CuZnAl layer with different voltages in range of 60 to 180 V for 4 minutes. Level of agglomeration is raised with increase in voltage. More inhomogeneity is reached with higher particles velocity during deposition [19]. As shown in Figure 9, methanol conversion is raised with increase in voltage from 60 to 140 V. It is clear that higher voltage effectively results in more weight of deposition in range of 60 to 140 V. Full methanol conversion was achieved at 270

°C for 140 V. Beside the weight of deposition, both porosity and cracking could result in the higher conversion due to developing effective diffusion factor [33]. In contrary, performance of 60 V and packed-bed resulted in lower conversion of 92 and 86 %, respectively, at 270 °C. In case of CO selectivity, 60 V and packed-bed represented 4.06 and 3.4 %, respectively, at 270 °C. The H_2 yield is ranged from about 66 to 99.9 % and it is increased as the applied voltage is raised. Finally, all voltages reach to 99.9 % at 270 °C.

Figure 10 shows the current density and weight of deposition for different voltages during 4 minutes. As expected, the current density is increased from 60 to 140 V due to raising electrical field. Moreover, slope of the current density is raised with increase in the voltage which represents force to particles during the time.

3.4 Effect of GHSV and S/C

The effect of gas hourly space velocity (GHSV) for MSR over catalytic coated plates are shown in Figure 11. The conditions of molar ratio of steam to methanol of 1.3:1 (S/C), and temperature of 270 °C were considered. The GHSV was varied from 12000 to 36000 h^{-1}. As shown in Figure 11, the methanol conversion is decreased with increase in GHSV, that it is attributed to decrease in the residence time of reactants over the catalytic bed which consequently lowers methanol conversion. The conversion is varied from 82.63 and 100% in the considered

range. However, there is no significant change for the H_2 and the CO_2 fractions but it strongly varies for the CO. It is obvious that increase in GHSV slightly lowers the H_2 yield from 99.9 to 97.73, while the GHSV is differed from 12000 to 36000 h^{-1}. The effect of S/C over the coated CuZnAl catalyst was investigated. As shown in Figure 12, methanol conversion significantly increases with a rise in S/C below 1.3, at 270 °C. In case of the fractions, the CO is decreased with increase in S/C. Volumetric fraction of CO is about 3.14% when the S/C is 0.7, and then is decreased to 0.64% with rising S/C to 2. According to the results, higher S/C is more favorable to reduce the CO content. Eq. (1) shows that the S/C of 1.0 will be stoichiometrically optimal for MSR. However, according to the Eq. (1) and (3), excess steam develops methanol conversion and decreases the CO content through shifting the water gas shift equilibrium rightward. Moreover, the system will be more cost-effective with lower steam due to the heating problems.

4 Conclusion

Regard to catalyst coating onto metal-based microreactors, further study takes into account alternatives to improve the procedure to gain more effectively. In an overview of this study, the interesting method of EPD was successfully performed to coat a CuZnAl layer onto stainless steel for methanol steam reforming. The optimal conditions of coating procedure was achieved by variation of physical-based parameters of time and voltage. The results showed that higher time of EPD

made more deposition to time of 4 minutes and then methanol conversion was decreased with increase in time of deposition. At the next step, regarding time of 4 minutes as optimum, variation of voltage (60-180 V) was evaluated. The results showed that increase in voltage to 140 V caused more deposition weight and roughness of surface. After that, no deposition was found with voltages higher than 140 V. The full methanol conversion was practically achieved at 140 V and time of 4 minutes. Coated and packed-bed types were compared, on which the performance of microreactor was better than quartz fixed bed.

References

[1] S. Hočevar, W. Summers, in: A. Léon (Ed.), Hydrogen Technology, Springer Berlin Heidelberg, 2008, pp. 15-79.

[2] F. Meshkani, M. Rezaei, RSC Advances 5 (2015) 9955-9964.

[3] C. Song, N. Brandon, D. Thompsett, Fuel Cells Compendium, Elsevier, Oxford, 2005.

[4] C.C. Shen, T.Y. Jian, Y.T. Wang, Fuel Cells 13 (2013) 965-970.

[5] A. Qi, B. Peppley, K. Karan, Fuel Processing Technology 88 (2007) 3-22.

[6] B.A. Peppley, J.C. Amphlett, L.M. Kearns, R.F. Mann, Applied Catalysis A: General 179 (1999) 21-29.

[7] V. Hessel, S. Hardt, H. Löwe, Chemical micro process engineering: fundamentals, modelling and reactions, John Wiley & Sons, 2006.

[8] V. Meille, Applied Catalysis A: General 315 (2006) 1-17.

[9] H. Hadraba, J. Klimes, K. Maca, Journal of materials science 42 (2007) 6404-6411.

[10] H. Hadraba, D. Drdlik, Z. Chlup, K. Maca, I. Dlouhy, J. Cihlar, Journal of the European Ceramic Society 32 (2012) 2053-2056.

[11] H. Akbulut, G. Hatipoglu, H. Algul, M. Tokur, M. Kartal, M. Uysal, T. Cetinkaya, Surface and Coatings Technology (2015).

[12] R. Nedyalkova, C. Torras, J. Salvadó, D. Montané, Fuel Processing Technology 91 (2010) 1040-1048.

[13] R. Nedyalkova, A. Casanovas, J. Llorca, D. Montané, international journal of hydrogen energy 34 (2009) 2591-2599.

[14] S. Majhi, S. Behura, S. Bhattacharjee, B. Singh, T. Chongdar, N. Gokhale, L. Besra, international journal of hydrogen energy 36 (2011) 14930-14935.

[15] J. Cherng, C. Wu, F. Yu, T. Yeh, Journal of Power Sources 232 (2013) 353-356.

[16] C. Felix, T.-C. Jao, S. Pasupathi, V.M. Linkov, B.G. Pollet, Journal of Power Sources 258 (2014) 238-245.

[17] Q. Chen, U.P. de Larraya, N. Garmendia, M. Lasheras-Zubiate, L. Cordero-Arias, S. Virtanen, A.R. Boccaccini, Colloids and Surfaces B: Biointerfaces 118 (2014) 41-48.

[18] A. Boccaccini, S. Keim, R. Ma, Y. Li, I. Zhitomirsky, Journal of The Royal Society Interface 7 (2010) S581-S613.

[19] L. Besra, M. Liu, Progress in materials science 52 (2007) 1-61.

[20] O.O. Van der Biest, L.J. Vandeperre, Annual Review of Materials Science 29 (1999) 327-352.

[21] C.-C. Chang, C.-T. Chang, S.-J. Chiang, B.-J. Liaw, Y.-Z. Chen, international journal of hydrogen energy 35 (2010) 7675-7683.

[22] S.R.G. Carrazán, R. Wojcieszak, R.M. Blanco, C. Mateos-Pedrero, P. Ruiz, Applied Catalysis B: Environmental 168 (2015) 14-24.

[23] K.-S. Lin, S. Chowdhury, H.-P. Yeh, W.-T. Hong, C.-T. Yeh, Catalysis Today 164 (2011) 251-256.

[24] Y. Matsumura, H. Ishibe, Applied Catalysis B: Environmental 91 (2009) 524-532.

[25] M.M. Günter, T. Ressler, R.E. Jentoft, B. Bems, Journal of Catalysis 203 (2001) 133-149.

[26] K.B. Singh, M.S. Tirumkudulu, Physical review letters 98 (2007) 218302.

[27] J. Agrell, H. Birgersson, M. Boutonnet, Journal of Power Sources 106 (2002) 249-257.

[28] J.K. Lee, J.B. Ko, D.H. Kim, Applied Catalysis A: General 278 (2004) 25-35.

[29] H. Purnama, T. Ressler, R.E. Jentoft, H. Soerijanto, R. Schlögl, R. Schomäcker, Applied Catalysis A: General 259 (2004) 83-94.

[30] X. Yu, S.-T. Tu, Z. Wang, Y. Qi, Journal of Power Sources 150 (2005) 57-66.

[31] R.-Y. Chein, Y.-C. Chen, Y.-S. Lin, J. Chung, International Journal of Thermal Sciences 50 (2011) 1253-1262.

[32] L. Yang, X. Wu, D. Weng, Colloids and Surfaces A: Physicochemical and Engineering Aspects 287 (2006) 16-23.

[33] V. Novák, P. Kočí, T. Gregor, J.-S. Choi, F. Štěpánek, M. Marek, Catalysis Today 216 (2013) 142-149.

List of Symbols

Subscripts

CO	Carbon Monoxide
CO_2	Carbon Dioxide
cat	Catalyst
e	Electrophoretic
hlk	Miller Index
H_2	Hydrogen
in	Inlet
MeOH	Methanol
out	Outlet

Script

BET	Brunauer-Emmett-Teller
cm	Centimeter
D.I	Deionized
FESEM	Field Emission Scanning Electron Microscope
GHSV	Gas Hourly Space Velocity
h	Hour
JCPDS	Joint Committee on Powder Diffraction Standards
kJ	Kilo Joule
L	Length
M	Molarity
ml	Milliliter
min	Minute
mm	Millimeter
nm	Nano Meter
rpm	revolutions per Minute
rWGS	Reverse Water Gas Shift
V	Voltage
W	Width
Wt	Weight

Figure Captions:

Figure 1. The micro channel reactor configuration.

Figure 2 .preparation steps of electrophoretic CuZnAl slurry and EPD set up.

Figure 3. XRD patterns of coated layers of the CuZnAl catalyst at 140 V, 4 minutes and 0.6 wt.% PEI.

Figure 4. FESEM images and reconstructed 3D view of coated layers for different time of EPD.

Figure 5. Weight deposition and methanol conversion vs. time and voltage.

Figure 6. Micro-reactor performance vs. time of EPD, S/C=1.3 and GHSV=23000 h^{-1}.

Figure 7. Current density and weight distribution vs. deposition time under 100 V.

Figure 8. FESEM images and reconstructed 3D view of coated layers for different voltages of EPD for 4 minutes.

Figure 9. Micro-reactor performance vs. voltage of EPD, S/C=1.3 and GHSV=23000 h^{-1}.

Figure 10. Current density and weight distribution vs. voltage for 4 minutes.

Figure 11. Micro-reactor performance for 140 V and time of 4 minutes vs. GHSV (h^{-1})

Figure 12. Micro-reactor performance for 140 V and time of 4 minutes vs. steam to methanol molar ratio.

Table Captions:

Table 1. Structural properties of CuZnAl catalyst in powder and coated layer state.

Table 2. Slurry composition for various EPD coating of CuZnAl catalyst.

Table 3. Comparison of packed-bed and coated configuration for MSR reaction.

Table 1. Structural properties of CuZnAl catalyst in powder and coated layer state.

Catalyst	**CuZnAl**	**CuZnAl**	**CuZnAl**
Sample	Powder	Coated- fresh	Coated-used
Chemical composition (ICP-OES)(Wt%)	38.69Cu 51.47Zn 9.83Al	-	-
Surface area ($m^2.g^{-1}$)	121	-	-
Pore volume ($cm^3.g^{-1}$)	0.488	-	-
Pore size (nm)	16.1	-	-
Crystallite size[a] (nm)	8.69	6.15	7.39
Lattice parameters (Aº)	a= 3.2452 b= 3.2452 c= 5.2951	a= 3.2348 b= 3.2348 c= 3.0713	a= 3.2384 b= 3.2384 c= 3.0749

[a] The scherre's equation was used.

Table 2. Slurry composition for various EPD coating of CuZnAl catalyst

Catalyst	EPD			Slurry			Coated layer
	Voltage (V)	Time (minute)	Electrodes Distance (mm)	Powder (%)	Binder (%)	Solvent (cc)	Deposition (mg)
CuZnAl	100	2	15	3	0.6	40	21
CuZnAl	100	4	15	3	0.6	40	37
CuZnAl	100	5	15	3	0.6	40	37
CuZnAl	140	4	15	3	0.6	40	48
CuZnAl	60	4	15	3	0.6	40	18
CuZnAl	180	4	15	3	0.6	40	0

Table 3. Comparison of packed-bed and coated configuration for MSR reaction.

Parameter	Micro reactor	Fixed-bed Reactor
Reaction Temperature (ºC)	270	270
Ar/Pump	33.33	33.33
S/C	1.3	1.3
GHSV (hr^{-1})	22000	22000
MeOH Conversion (%)	100	86
H_2 Yield (%)	99.9	99.9
CO_2 Selectivity (%)	95.08	96.59
CO Selectivity (%)	4.91	3.40
Catalyst Loading (mg)	96	100
Particle size (µm)	Less than 37	250-420

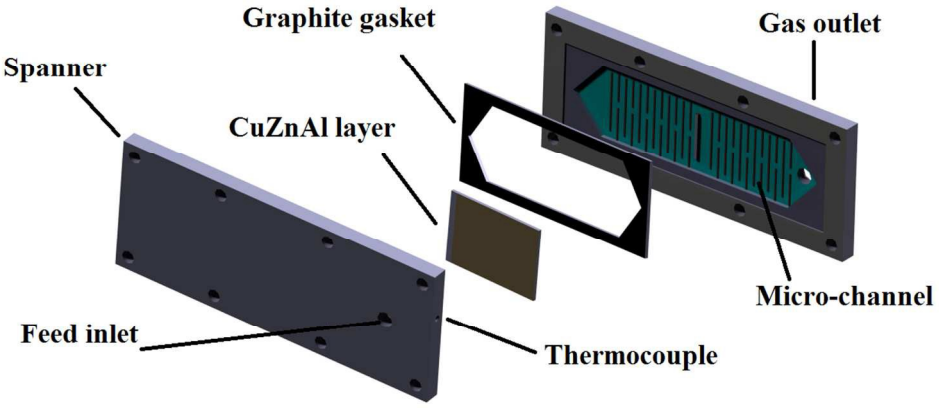

Figure 1. The micro channel reactor configuration.
346x150mm (96 x 96 DPI)

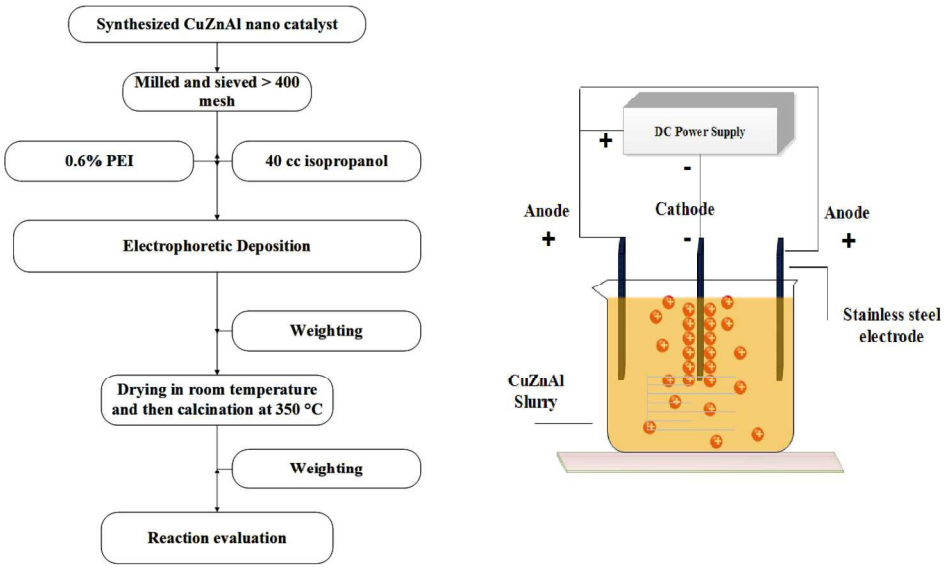

Figure 2 .preparation steps of electrophoretic CuZnAl slurry and EPD set up.
946x529mm (96 x 96 DPI)

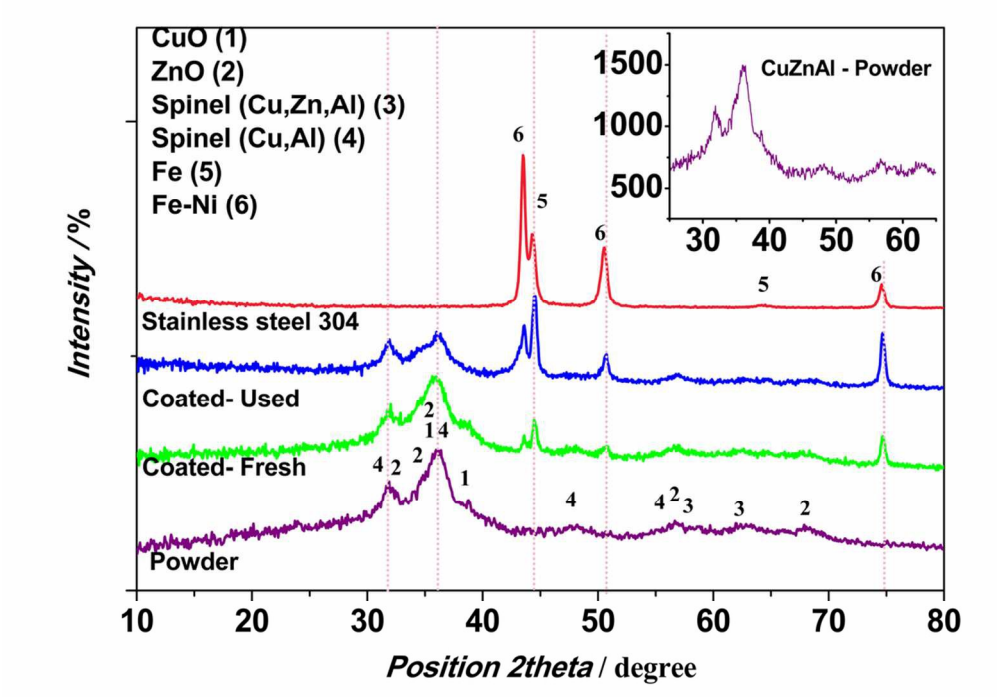

Figure 3. XRD patterns of coated layers of the CuZnAl catalyst at 140 V, 4 min and 0.6 wt.% PEI.
50x35mm (600 x 600 DPI)

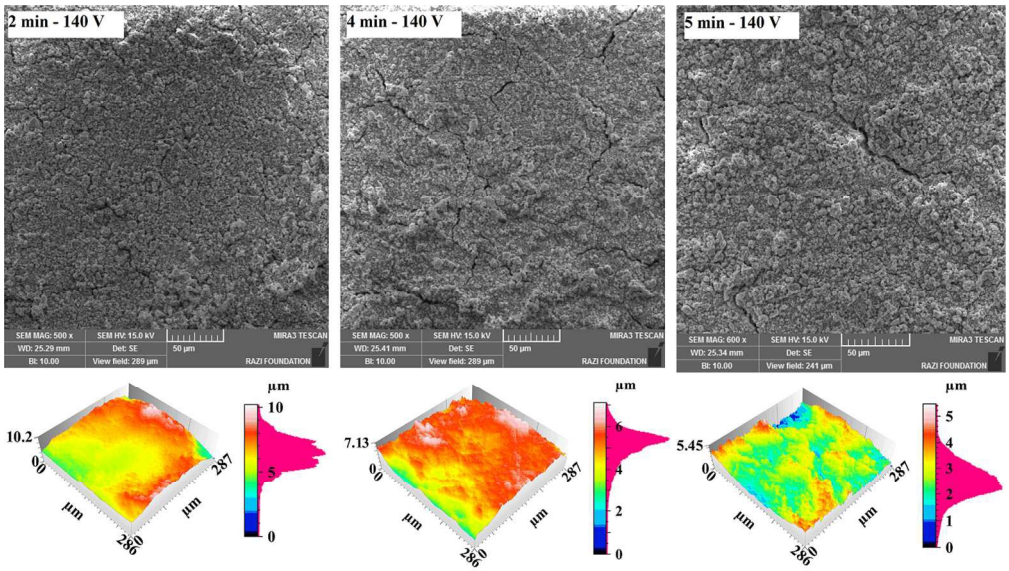

416x238mm (96 x 96 DPI)

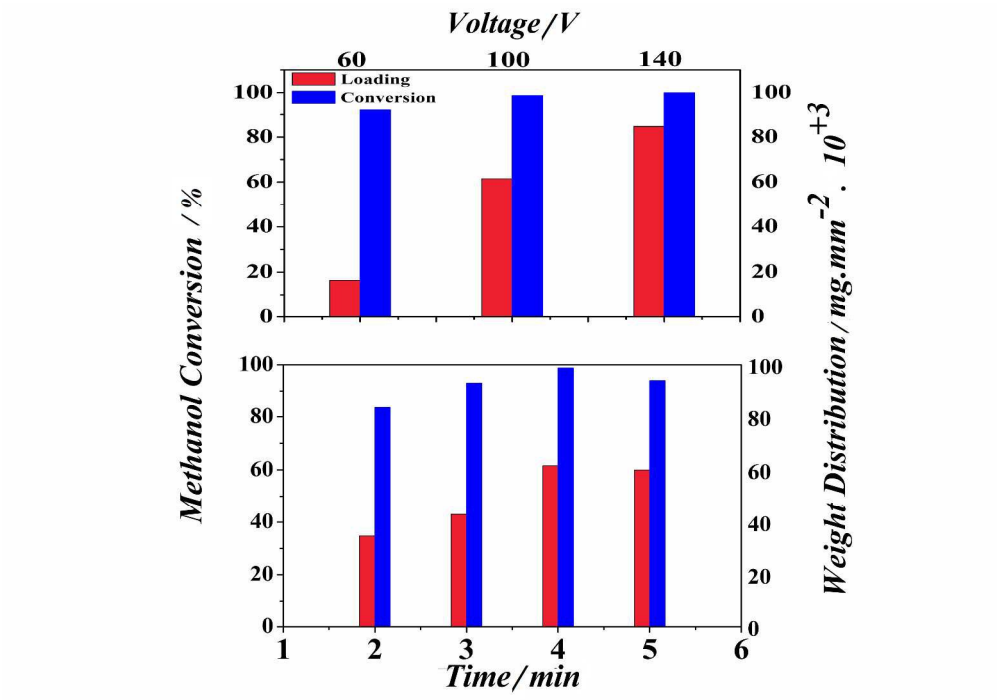

Figure 5. Weight deposition and methanol conversion vs. time and voltage.
896x630mm (96 x 96 DPI)

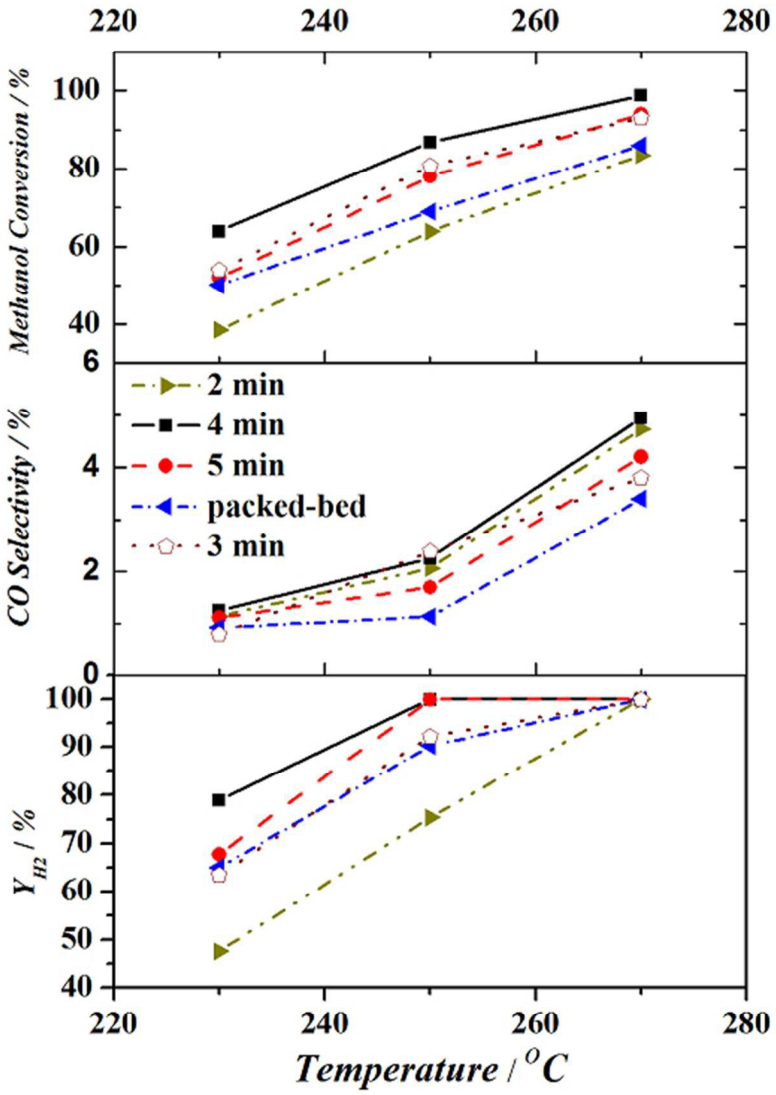

143x204mm (100 x 100 DPI)

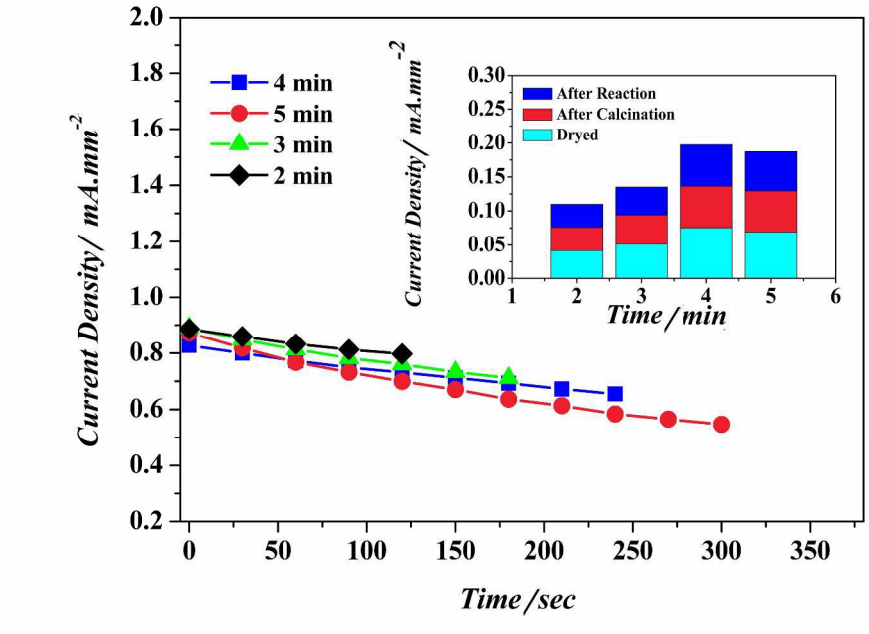

Figure 7. Current density and weight distribution vs. deposition time under 100 V.
896x629mm (96 x 96 DPI)

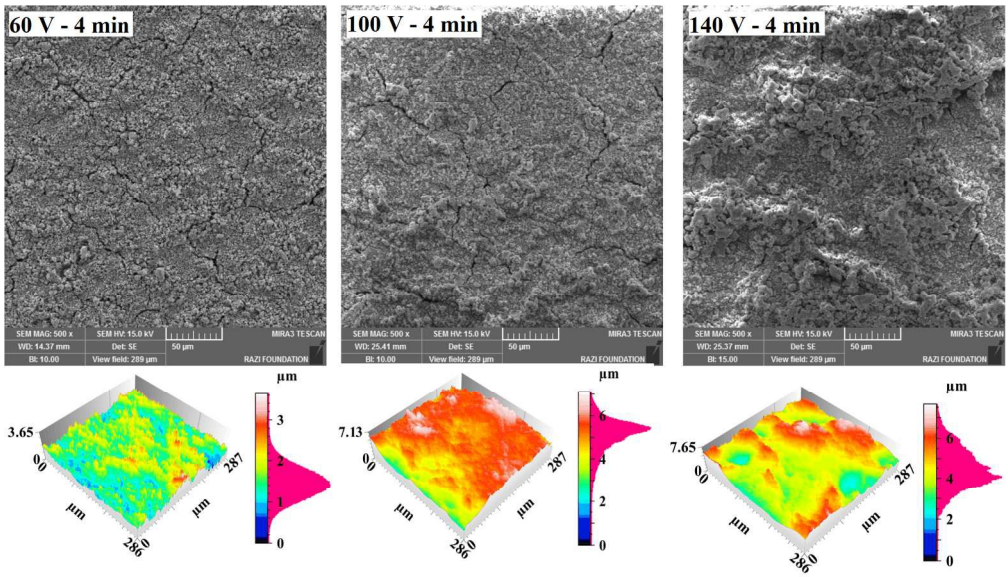

552x319mm (96 x 96 DPI)

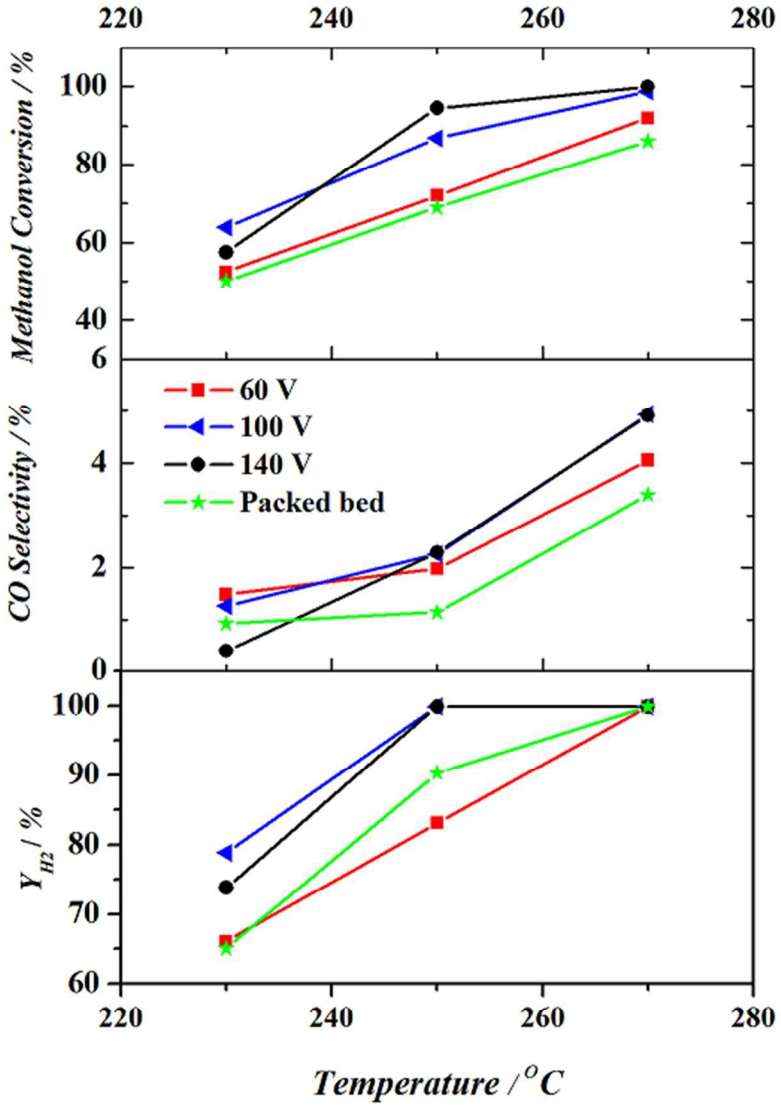

143x204mm (100 x 100 DPI)

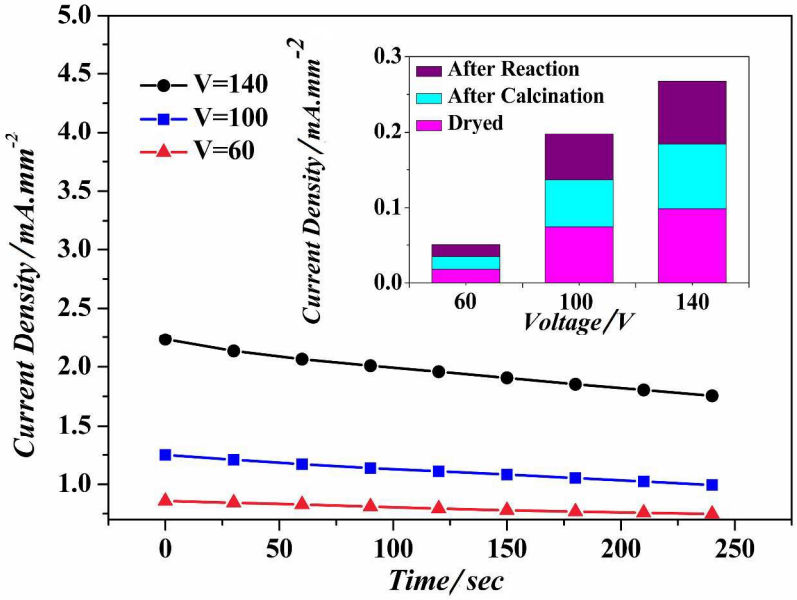

Figure 10. Current density and weight distribution vs. voltage for 4 min.
896x630mm (96 x 96 DPI)

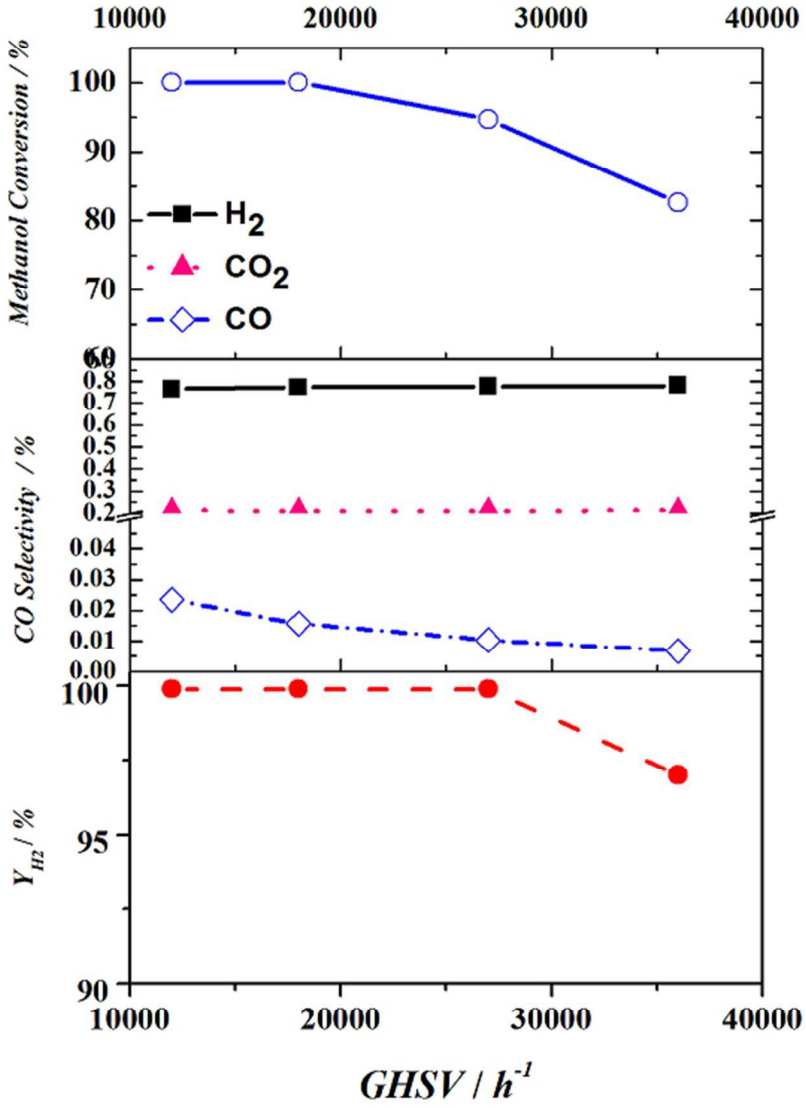

143x204mm (100 x 100 DPI)

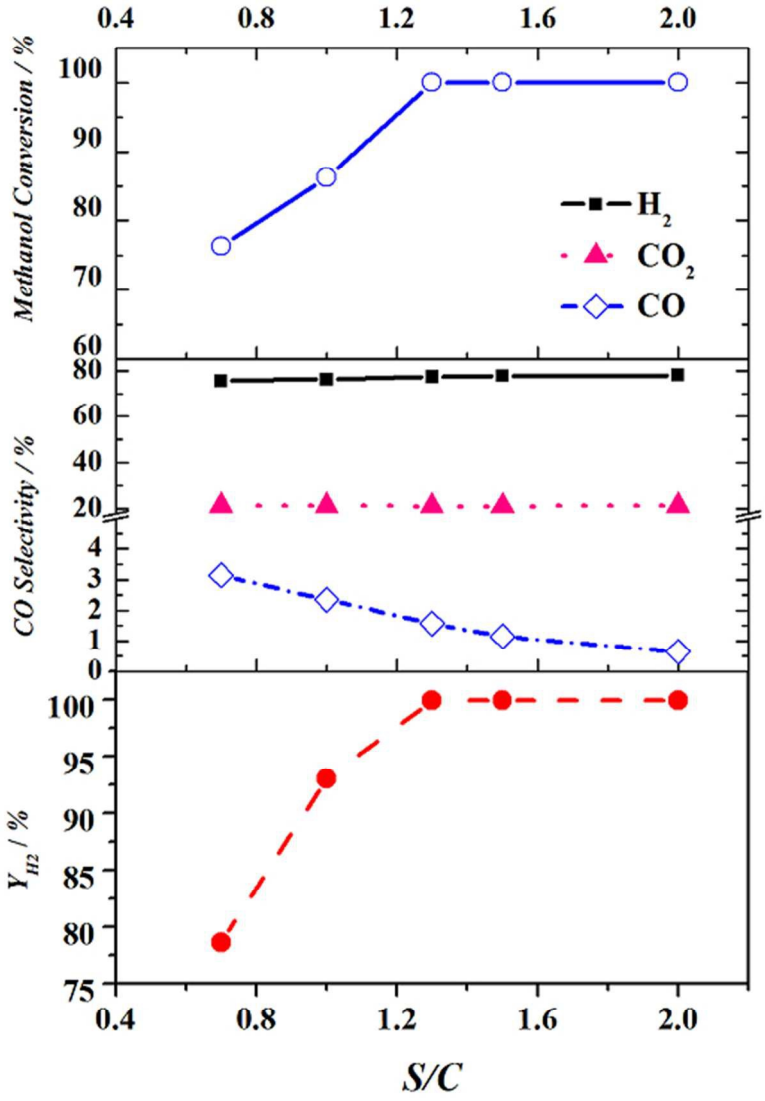

143x204mm (100 x 100 DPI)

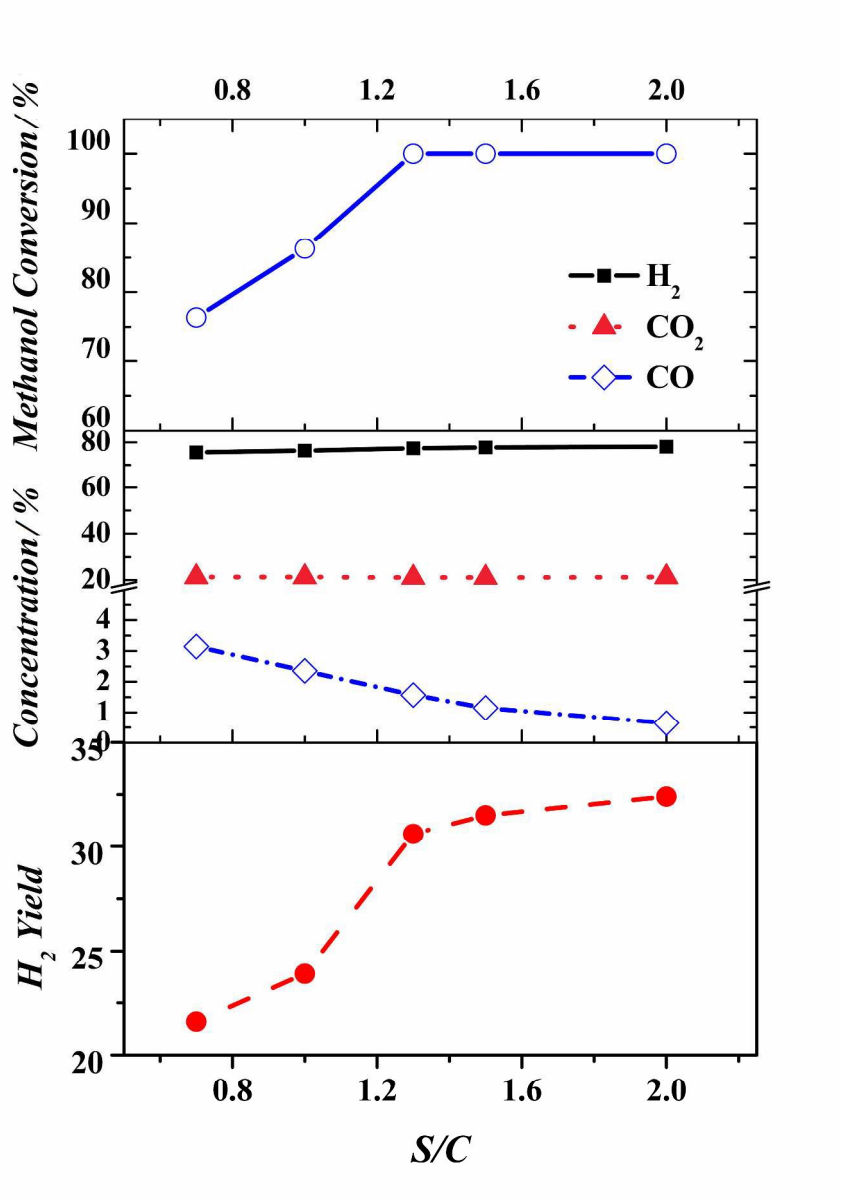

Figure 12. Micro-reactor performance for 140 V and time of 4 min vs. steam to methanol molar ratio.
807x1149mm (96 x 96 DPI)

"Metal microreactor coated with EPD technique is an alternative strategy to improve catalyst performance by optimization of physical coating parameters."

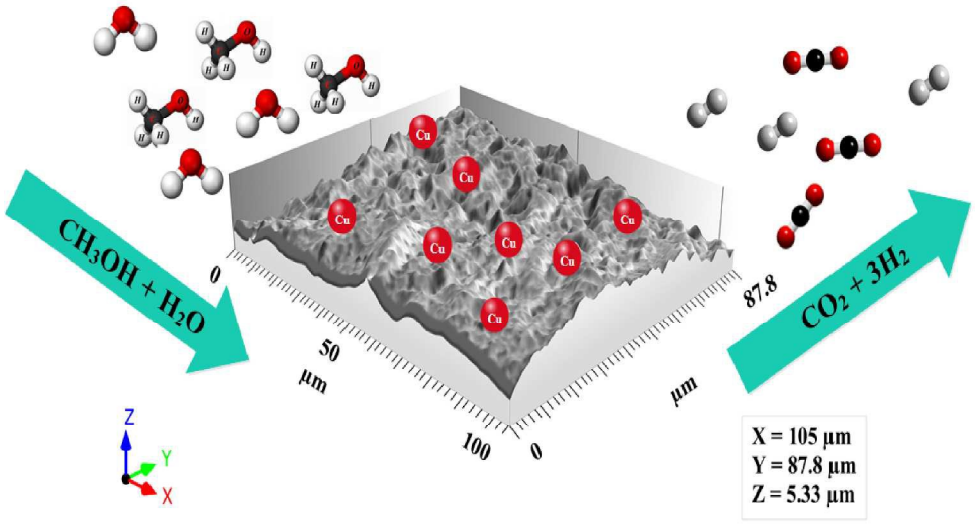

944x673mm (96 x 96 DPI)